ACS APPLIED MATERIALS & INTERFACES

Research Article

www.acsami.org

Engineering of the Chemical Reactivity of the Ti/HfO_2 Interface for RRAM: Experiment and Theory.

Pauline Calka,*[,†] Malgorzata Sowinska,[†] Thomas Bertaud,[†] Damian Walczyk,[†] Jarek Dabrowski,[†] Peter Zaumseil,[†] Christian Walczyk,[†] Andrei Gloskovskii,[‡] Xavier Cartoixà,[§] Jordi Suñé,[§] and Thomas Schroeder[†,∥]

[†]IHP, Im Technologiepark 25, 15236 Frankfurt an der Oder, Germany

[‡]Deutsches Elektronen-Synchrotron (DESY), 22607 Hamburg, Germany

[§]Departament d'Enginyeria Electrònica, Universitat Autònoma de Barcelona, 08193 Bellaterra, Spain

[∥]Brandenburgische Technische Universität, Konrad-Zuse-Strasse 1, 03046 Cottbus, Germany

ABSTRACT: The Ti/HfO_2 interface plays a major role for resistance switching performances. However, clear interface engineering strategies to achieve reliable and reproducible switching have been poorly investigated. For this purpose, we present a comprehensive study of the Ti/HfO_2 interface by a combined experimental−theoretical approach. Based on the use of oxygen-isotope marked Hf^*O_2, the oxygen scavenging capability of the Ti layer is clearly proven. More importantly, in line with ab initio theory, the combined HAXPES-Tof-SIMS study of the thin films deposited by MBE clearly establishes a strong impact of the HfO_2 thin film morphology on the Ti/HfO_2 interface reactivity. Low-temperature deposition is thus seen as a RRAM processing compatible way to establish the critical amount of oxygen vacancies to achieve reproducible and reliable resistance switching performances.

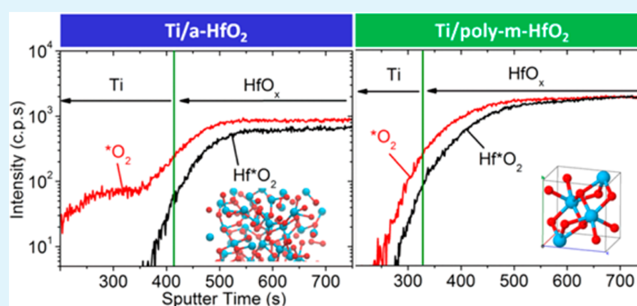

KEYWORDS: *RRAM, Ti/HfO_2, oxygen vacancy stability, oxygen diffusion, amorphous HfO_2, reliability*

1. INTRODUCTION

With low-power dissipation, resistive RAM (RRAM) technology is well suited to address high-end embedded non-volatile memory (NVM) applications, such as wireless sensor networks[1] and bio-inspired neuromorphic systems.[2] Devices consist of metal−insulator−metal (MIM) structures whereby the memory effect occurs via insulator resistance switching (RS) between a high and a low resistance state under bias. In the case of transition metal oxide-based RRAM, RS relies on the drift of oxygen vacancies initially present in the oxide or produced during the first RS.[3,4] Structural phase changes,[5] nanoionic valence changes,[3] and lattice disorder[6] can also be involved. Details of the physical mechanism are still debated. The next bottleneck is to use this knowledge to improve both control of the RS parameters and reliability. Thus, controlled nanoscale manipulation of defects is urgently needed. In terms of materials, HfO_2 is a very interesting candidate because it combines the advantages of CMOS compatibility and promising performances.[7] Better control of the RS was achieved for HfO_2-based devices by introducing defects using a thin Ti oxygen getter capping layer.[8,9] Highly reliable HfO_2-based resistive memory, which adopts Ti as the oxygen gettering layer to form TiO_X/HfO_X, have been achieved with excellent endurance ($>10^6$ cycles), suitable retention (10 years at 200 °C) and high ON/OFF resistance ratio (>1000).[8] Another interesting property of the Ti/HfO_2 interface is lowered power dissipation. Forming voltage (V_F) and set voltage can be drastically reduced. For instance, in $TiN/HfO_2/Pt$ structures V_F is 3.75 V, whereas V_F is 1.9 V for $TiN/HfO_2/Ti$.[9] In addition, the importance of the Ti layer position and thickness has been shown.[10,11] These studies point out the crucial role of interface control over device performances. It is important now to outline clear strategies for engineering the Ti/HfO_2 interface physical and chemical properties to achieve reproducible and reliable RRAM performance.

In this work, we unveil the chemical reactivity of the Ti/HfO_2 interface as a function of HfO_2 thin film morphology with a comprehensive study including experimental measurements and theoretical calculations. Thin films have been deposited using molecular beam epitaxy (MBE), offering ultra-high vacuum (UHV), which is critical to avoid background oxidation of the Ti layer and thus directly trace the oxygen scavenging activity of Ti deposited on HfO_2. Ti deposition over HfO_2 is directly monitored by in situ X-ray photoelectron spectroscopy (XPS) in the MBE chamber. A model correlating the data is used to extract the growth mode of Ti. Time-of-flight secondary ion mass spectrometry (ToF-SIMS) performed on HfO_2 containing an oxygen isotope (*O) allows to extract oxygen

Received: January 9, 2014
Accepted: March 13, 2014
Published: March 13, 2014

 © 2014 American Chemical Society

diffusion profiles characteristic from the Ti/HfO_2 interactions by disentangling oxide and environmental contribution. More specifically we used the oxygen isotope ^{18}O (natural abundance = 0.2%). Hard X-ray photoelectron spectroscopy (HAXPES) is used in order to record non-destructively the chemical bonding at the buried interface. Finally, the oxygen diffusion at the Ti/HfO_2 interface depending on HfO_2 morphology is corroborated by theoretical calculations.

2. EXPERIMENTAL SECTION

Ti/HfO_2/TiN samples were produced by MBE deposition of Ti/HfO_2 on polycrystalline TiN(73 nm)/Si(001) substrates. HfO_2, containing the abundant oxygen isotope *O, and Ti were deposited consecutively in the same MBE chamber. Metallic Hf was evaporated in an $*O_2$ background ($p = 10^{-5}$ mbar), then, after a N_2 purge, metallic Ti was evaporated. The HfO_2 thin films were deposited either at room temperature or at 400 °C; the Ti layer was deposited subsequently at room temperature for all the samples. Ti growth on HfO_2 (21 nm) was monitored in a neighboring chamber, without breaking vacuum, using in situ XPS. Deposition time was tuned for the formation of a continuous Ti layer (about 11 nm thick), as explained in the results part. The impact of Hf oxide morphology on Ti/HfO_2 interactions was investigated using complementary characterization techniques: grazing incidence x-ray diffraction (GIXRD), Tof-SIMS and HAXPES. In situ XPS was carried out using an Al Kα (1486.6 eV) source and a Specs Phoibos 100 hemispherical energy analyzer with a collection angle of 45° with respect to the surface normal. The escape depth was 1.8 nm assuming an inelastic mean free path (IMFP)[12] of 2.6 nm for the Hf $4d_{5/2}$ (214 eV) photoelectrons through Ti. HAXPES experiments were carried out at the beamline P09 of PETRA III storage ring at DESY (Hamburg, Germany). Photoelectrons excited at 8 keV using a Si(311) double-crystal monochromator were collected with a SPECS Phoibos 225 HV spectrometer under a collection angle of 7°. The corresponding escape depth was 11.2 nm, taking into account an IMFP[12] (Hf $4d_{5/2}$) of 11.3 nm. These conditions allowed measuring the chemical states of interfacial Ti non-destructively. Binding energy calibration was performed using Au 4*f*.

3. RESULTS AND DISCUSSION

3.1. Growth of Ti on HfO_2.

First, the growth mode of Ti on HfO_2 is investigated using in situ XPS to determine the deposition conditions for producing a continuous overlayer. A first insight into oxidation states is also given. Figures 1 and 2 present the results obtained for the Ti/HfO_2 sample with hafnium oxide deposited at room temperature (RT). Ti deposition is monitored step by step in the MBE chamber for times up to 1500 s. Figure 1 presents the photoelectron spectra of the Ti 2*p* and Hf 4*d* core levels measured after 10, 20, and 240 s. After the Shirley background subtraction, the decomposition of the Ti 2*p* photoelectron peak was performed using Gaussian−Lorentzian functions for the oxide components and a Doniach−Sunjic function for the metallic component.

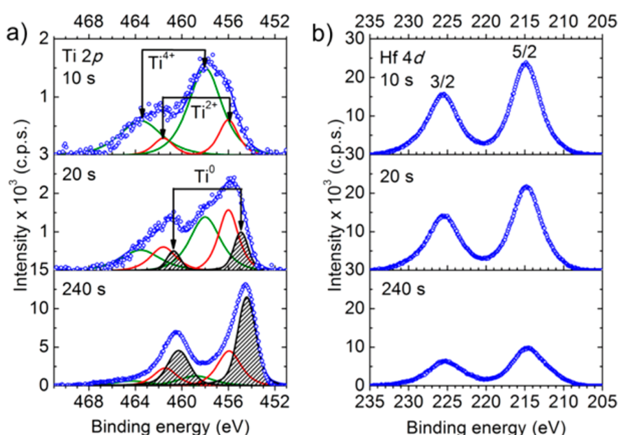

Figure 1. Photoelectron spectra of the Ti 2*p* (a) and Hf 4*d* (b) electronic core levels measured by in situ XPS after MBE deposition of Ti on HfO_2(RT). Data are displayed for three deposition times.

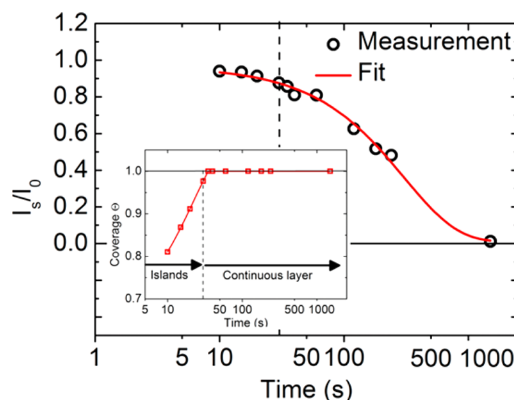

Figure 2. Intensity ratio (circles) of Hf 4*d* photoelectron monitored by in situ XPS, during (I_s) and before (I_0) Ti deposition on HfO_2(RT), depending on Ti deposition time. Experimental data are compared to the theoretical signal attenuation of the Volmer−Weber growth mode (red line). Inset: Phases of the Ti growth on HfO_2 extracted from the measurements.

A clear evolution of the Ti 2*p* photoelectron spectra is observed over time. After 10 s, only Ti oxidized states (2+ and 4+) are measured. With increasing deposition time, metallic Ti^0 starts to form around 20 s, and after 240 s, the peak slightly shifts to lower binding energies, probably because of the cluster size effects.[13] The buried Ti/HfO_2 interface has therefore an enhanced chemical reactivity with oxygen towards the Ti overlayer. At this point, it is however difficult to give a final conclusion on the origin of the oxygen atoms. Oxygen is present in HfO_2 and at low concentration in the MBE chamber (10^{-9} mbar); therefore complementary analysis (using *O profile) to disentangle both contribution are presented further, below. By tracking the attenuation of the Hf $4d_{5/2}$ signal (I_s) compared to initial Hf $4d_{5/2}$ signal (I_0) before Ti deposition, see Figure 1, the Ti overlayer growth is traced in situ. The experimental data are compared to the theoretical intensity attenuation for the Volmer−Weber (or 3D) growth:[14]

$$I_s(t) = I_0[1 - \Theta(t)] + I_0\Theta(t)\exp[-h/\lambda \cos\theta] \quad (1)$$

where $\Theta(t)$ measures the surface coverage (from 0 to 1), λ is the IMFP of the Hf $4d_{5/2}$ photoelectrons through Ti, θ is the photoelectrons collection angle and h is the average thickness of the deposited material. I_s/I_0 is plotted as a function of time (t) in Figure 2. There is a good agreement between simulation and experimental data, indicating that the Ti deposition over HfO_2 corresponds to the Volmer−Weber growth mode. Ti atoms are initially poorly bounded to the substrate, thus TiO islands nucleate and expand three dimensionally in all directions. Finally, the islands, becoming more and more metallic, coalesce and a closed layer forms after 30 s deposition (inset of Figure 2). Consequently, growth deposition times well above 1000 s are used in the following buried Ti/HfO_2 interface studies to assure closed Ti layers.

3.2. Ti/HfO_2 Physics and Chemistry Depending on HfO_2 Morphology.

The oxygen diffusion in the Ti/HfO_2

dx.doi.org/10.1021/am500137y | ACS Appl. Mater. Interfaces 2014, 6, 5056−5060

stack is now investigated in detail for both RT and 400°C oxygen isotope marked Hf*O_2 with a closed Ti overlayer. Figure 3 displays the results obtained for HfO_2(RT). The

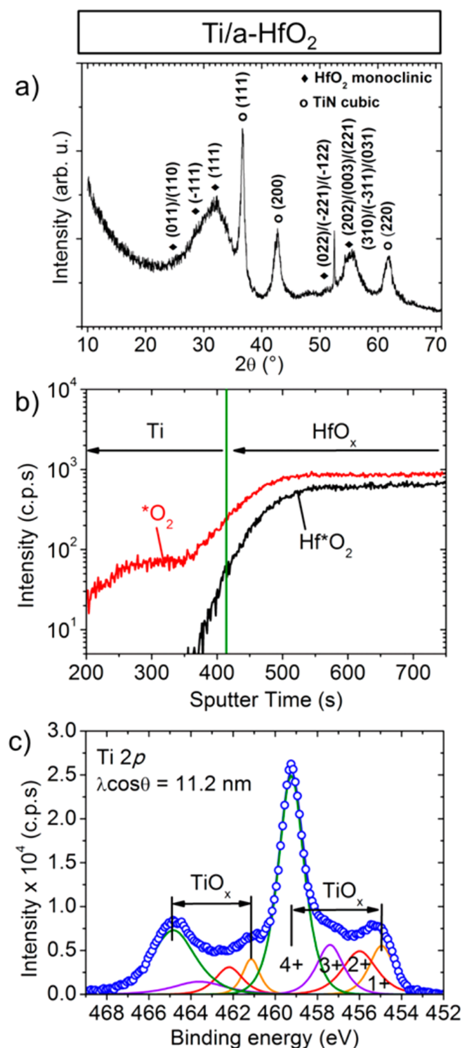

Figure 3. Material characterizations performed on Ti/HfO_2 (RT) using (a) GIXRD, (b) Tof-SIMS, and (c) HAXPES. The use of marked oxygen *O allows to discuss oxygen diffusion from Hf to Ti unambiguously by eliminating environmental contributions.

GIXRD measurement (Figure 3a) shows three broad peaks attributed to hafnium oxide around 30°, 50°, and 55°. The one at 30° corresponds to a bunch of reflections from the monoclinic lattice: (011) or (110) at 24.5°, (−111) at 28.5°, and (111) at 31.5° (ICDD no. 00-034-0104). In our measurements, these peaks are broadened and form a single component, indicating the formation of amorphous hafnium oxide containing only small crystallites in the monoclinic phase. The two other components present at higher angles (50° and 55°) correspond to a number of reflections of the monoclinic lattice as well (ICDD no. 00-034-0104), as indicated in Figure 3a. These reflections are so close to one another that they cannot be well resolved for poorly crystalline, mostly amorphous thin films. Figure 3b presents the oxygen isotope profile performed by Tof-SIMS. Clearly, the broad shoulder at smaller sputter time indicates that oxygen is present in the Ti overlayer and that *O diffused from HfO_2. Further, the impact of oxygen diffusion on Ti oxidation states is studied non-destructively by HAXPES. The Ti 2*p* photoelectron spectrum was recorded for interfacial Ti (Figure 3c). The data are modeled as described in our former work.[15] At the interface, Ti is fully oxidized. Thus, both Tof-SIMS and HAXPES data confirm the enhanced reactivity of the interface suggested by the in situ XPS study (Figure 1). In particular, the use of oxygen isotope marked Hf*O_2 allows to clearly prove the oxygen scavenging capability of the Ti adlayer from the Hf*O_2 thin film.

The impact of hafnium oxide deposition temperature and crystallinity on the chemical reactivity of the Hf*O_2 interface is now investigated. Figure 4 presents results obtained for the Ti/

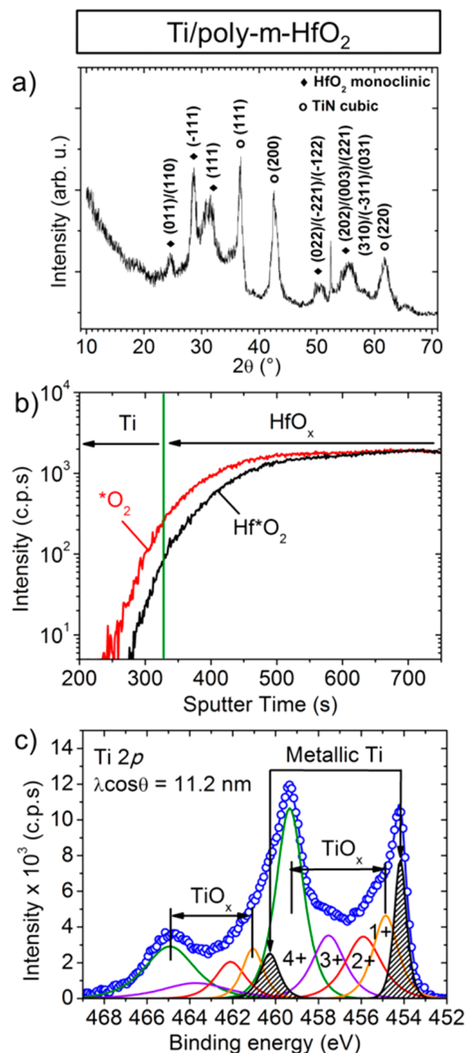

Figure 4. Material characterizations performed on Ti/HfO_2 (400°C) using (a) GIXRD, (b) Tof-SIMS, and (c) HAXPES.

HfO_2 sample with hafnium oxide deposited at 400 °C. The diffraction spectrum, in Figure 4a, shows that hafnium oxide fully crystallizes in the monoclinic phase. The peaks corresponding to the monoclinic lattice reflections (011)/(110) at 24.5°, (−111) at 28.5°, and (111) at 31.5° (ICDD no. 00-034-0104) are well-defined, as opposed to Figure 3a. Contrarily to Figure 3b, the *O profile in Figure 4b presents an abrupt drop by going from HfO_2 to Ti indicating that oxygen diffusion is limited to the first metallic interface layers only. Finally, titanium oxidation states are measured at the

dx.doi.org/10.1021/am500137y | ACS Appl. Mater. Interfaces 2014, 6, 5056−5060

interface non-destructively by HAXPES (Figure 4c). Metallic and oxidized titanium states are clearly observed, but most importantly, a clear difference with Figure 3c is visible, confirming that Ti oxidizes far less than in the previous mostly amorphous RT-Hf*O_2. Interestingly, our Tof-SIMS and HAXPES measurements show that HfO_2 morphology substantially controls the Ti/HfO_2 interface reactivity.

To obtain a microscopic insight into our results, we have performed first-principle calculations of the charged oxygen vacancy formation energies in the monoclinic (m-HfO_2) and amorphous (a-HfO_2) phase of hafnium oxide using the SIESTA package.[16] This code implements the density functional theory (DFT) in its generalized gradient approximation (GGA), using the parametrization for the exchange-correlation energy by Perdew−Burke−Ernzerhof.[17] We use norm-conserving pseudopotentials for the core electrons and a single-ζ plus polarization (SZP) basis set for the valence electrons, which gives a good compromise between accuracy, the obtained lattice parameters for m-HfO_2 (Figure 5a) are 5.149, 5.185, and 5.296 Å (5.117, 5.175, and 5.291 Å, experimentally[18,19]), and computational cost. The amorphous HfO_2 structure, containing 201 atoms (cf., Figure 5b), has been generated by a melt/quench cycle with the GULP molecular dynamics program,[20,21] followed by a structural relaxation with SIESTA until the force on each atom was less than 0.04 eV/Å.

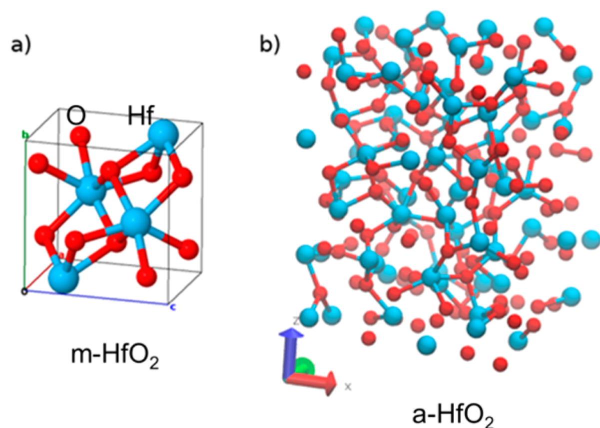

Figure 5. Ball-and-stick plots of the simulated (a) monoclinic (primitive cell) and (b) amorphous HfO_2.

The formation energies of (charged) vacancies, $\Delta E_{\mathrm{form}}^{V,q}$, are computed as differences in the total energies between the configuration with the oxygen removed and going to the molecular phase (reference chemical potential), with the electrons going to (coming from) the Fermi level, and the pristine state

$$\Delta E_{\mathrm{form}}^{V,q} = E^{V,q} - E^{\mathrm{pristine}} + \frac{1}{2}\mu_{O_2} + q(\varepsilon_{\mathrm{TVB}} + \mu_{\mathrm{F}}) \quad (2)$$

where $E^{V,q}$ is the energy of the system with a vacancy with charge q, E^{pristine} is the energy of the system without the vacancy, μ_{O_2} is the energy of molecular oxygen, and μ_{F} is the position of the Fermi level with respect to the top of the valence band, $\varepsilon_{\mathrm{TVB}}$. Spurious contributions to the total energy in systems with a net charge arising from the use of periodic boundary conditions are removed by the Makov−Payne[22] procedure, where we have properly accounted for the use of non-cubic cells and possibly anisotropic/tensor dielectric constants, as described in our previous work.[23]

Table 1 displays the oxygen vacancy formation energies for different charge states (eq 2), for the threefold coordinated O in monoclinic HfO_2 and three different oxygens in the amorphous structure. We observe that, in accordance with previous calculations, the vacancy is slightly less costly to create in the amorphous case,[24] which is to be expected given the metastability of the amorphous structure. Also in accordance with previous theoretical results,[25] the +2 charge state vacancy is strongly favored at low Fermi levels. Now, more importantly, Table 1 also shows that in the amorphous structures the formation of charged vacancies is energetically favored both in respect to (a) its crystalline counterpart and (b) its neutral equivalent, in agreement with our experimental results. Note that in some cases the charge vacancy formation energy is negative, implying a thermodynamically favored process. When looking at the intermediate steps for the structural relaxation, we observed that, in some cases for charged vacancies, heavy restructuration took place after removal of the oxygen atom, which we believe is the cause for the dramatic decrease in formation energies for those cases (i.e. the final state has a much reduced total energy becaue of the large atomic rearrangement).

Table 1. Oxygen Vacancy Formation Energies, with the Fermi Level at the Top of the Valence Band, for the Threefold Oxygen in Monoclinic HfO_2 and Oxygens at Three Different Positions (Randomly Chosen) in the Amorphous HfO_2 Host

	O vacancy formation energy (eV)			
vacancy charge	m-HfO_2	O(1) a-HfO_2	O(2) a-HfO_2	O(3) a-HfO_2
0	7.94	7.26	7.48	6.61
+1	5.92	7.25	1.69	−0.63
+2	4.04	−2.74	2.45	3.91

4. CONCLUSIONS

In summary, we provided a comprehensive experimental and theoretical study on Ti/HfO_2 interactions for RRAM applications. Thin films were deposited by MBE. First, room temperature Ti growth mode on HfO_2 was investigated. The Ti layer is fully closed after 30 s deposition time and the Ti/HfO_2 interface is clearly oxidized. Second, the physical and chemical interactions between the continuous Ti overlayer and HfO_2 depending on the oxide morphology were addressed. To disentangle influence by oxygen from the atmosphere, an oxygen isotope marked Hf*O_2 film was used to trace the oxygen diffusion. Two cases were studied: (a) Ti/a-HfO_2 (RT) and (b) Ti/poly-m-HfO_2 (400 °C). Clearly, Ti scavenges *O from hafnium oxide and therefore plays a major role for oxygen vacancy based RS. Finally, HfO_2 deposition conditions impacts Ti/HfO_2 reactivity because of HfO_2 film morphology. Metastable a-HfO_2 is more prone to maximize oxygen vacancy concentration. Thus, low temperature deposition of a-HfO_2 turns out as powerful approach to engineer the reactivity of the Ti/Hf*O_2 interface in order to create the initial amount of defects for reproducible and reliable RS performance.

AUTHOR INFORMATION

Corresponding Author

*E-mail: calka@ihp-microelectronics.com.

Notes

The authors declare no competing financial interest.

■ ACKNOWLEDGMENTS

IHP authors gratefully acknowledge the financial support from the Deutsche Forschungsgemeinschaft (DFG) for the RRAM project under contract SCHR 1123/7-1. P.C. is grateful to AvH foundation for granting an AvH PostDoc fellowship. X.C. and J.S. acknowledge support from the Spanish MINECO under grant No. TEC2012-32305 (partially supported by the EU under the FEDER Program), and DURSI of the Generalitat de Catalunya under contract 2009SGR783. J.S. also thanks the funding support of the ICREA ACADEMIA Award.

■ REFERENCES

(1) Zhang, K. *Embedded Memories for Nano-Scale VLSIs*, 1st ed; Springer Publications: New York, 2009.

(2) Yu, S.; Gao, B.; Fang, Z.; Yu, H.; Kang, J.; Wong, H. S. P. A Low Energy Oxide-Based Electronic Synaptic Device for Neuromorphic Visual Systems with Tolerance to Device Variation. *Adv. Mater.* **2013**, *25*, 1774−1779.

(3) Waser, R. *Nanoelectronics and Information Technology*, 3rd ed; Wiley-VCH Publications: Berlin, 2012.

(4) Gonon, P.; Mougenot, M.; Vallée, C.; Jorel, C.; Jousseaume, V.; Grampeix, H.; El Kamel, F. Resistance Switching in HfO_2 Metal−Insulator−Metal Devices. *J. Appl. Phys.* **2010**, *107*, No. 074507.

(5) Xue, K.-H.; Blaise, P.; Fonseca, L. R. C.; Nishi, Y. Prediction of Semimetallic Tetragonal Hf_2O_3 and Zr_2O_3 from First Principles. *Phys. Rev. Lett.* **2013**, *110*, No. 065502.

(6) Calka, P.; Martinez, E.; Delaye, V.; Lafond, D.; Audoit, G.; Mariolle, D.; Chevalier, N.; Grampeix, H.; Cagli, C.; Jousseaume, V.; Guedj, C. Chemical and Structural Properties of Conducting Nanofilaments in TiN/HfO_2-Based Resistive Switching Structures. *Nanotechnology* **2013**, *24*, No. 085706.

(7) Chen, Y. S.; Lee, H. Y.; Chen, P. S.; Tsai, C. H.; Gu, P. Y.; Wu, T. Y.; Tsai, K. H.; Sheu, S. S.; Lin, W. P.; Lin, C. H.; Chiu, P. F.; Chen, W. S.; Chen, F. T.; Lien, C.; Tsai, M. J. Challenges and Opportunities for HfO_x Based Resistive Random Access Memory. *IEEE Int. Electron Devices Meet.* **2011**, 31.3.1−31.3.4.

(8) Lee, H. Y.; Chen, P. S.; Wu, T. Y.; Chen, Y. S.; Wang, C. C.; Tzeng, P. J.; Lin, C. H.; Chen, F.; Lien, C. H.; Tsai, M. J. Low Power and High Speed Bipolar Switching with a Thin Reactive Ti Buffer Layer in Robust HfO_2 Based RRAM. . *IEEE Int. Electron Devices Meet.* **2008**, 1−4.

(9) Cagli, C.; Buckley, J.; Jousseaume, V.; Cabout, T.; Salaun, A.; Grampeix, H.; Nodin, J. F.; Feldis, H.; Persico, A.; Cluzel, J.; Lorenzi, P.; Massari, L.; Rao, R.; Irrera, F.; Aussenac, F.; Carabasse, C.; Coue, M.; Calka, P.; Martinez, E.; Perniola, L.; Blaise, P.; Fang, Z.; Yu, Y. H.; Ghibaudo, G.; Deleruyelle, D.; Bocquet, M.; Muller, C.; Padovani, A.; Pirrotta, O.; Vandelli, L.; Larcher, L.; Reimbold, G.; de Salvo, B. Experimental and Theoretical Study of Electrode Effects in HfO_2 Based RRAM. *IEEE Int. Electron Devices Meet.* **2011**, 28.7.1−28.7.4.

(10) Chen, P. S.; Lee, H. Y.; Chen, Y. S.; Gu, P. Y.; Chen, F.; Tsai, M. J. Impact of Engineered Ti Layer on the Memory Performance of HfO_x-Based Resistive Memory. *Electrochem. Solid-State Lett.* **2010**, *13*, H423−H425.

(11) Walczyk, C.; Wenger, C.; Walczyk, D.; Lukosius, M.; Costina, I.; Fraschke, M.; Dabrowski, J.; Fox, A.; Wolansky, D.; Thiess, S.; Miranda, E.; Tillack, B.; Schroeder, T. On The Role of Ti Adlayers for Resistive Switching in HfO_2-Based Metal-Insulator-Metal Structures: Top Versus Bottom Electrode Integration. *J. Vac. Sci. Technol., B: Nanotechnol. Microelectron.: Mater., Process., Meas., Phenom.* **2011**, *29*, No. 01AD02.

(12) Tanuma, S.; Powell, C. J.; Penn, D. R. Calculations of Electron Inelastic Mean Free Paths. V. Data for 14 Organic Compounds Over the 50−2000 eV Range. *Surf. Interface Anal.* **1994**, *21*, 165−176.

(13) Shukla, S.; Seal, S. Cluster Size Effect Observed for Gold Nanoparticles Synthesized by Sol-Gel Technique as Studied by X-ray Photoelectron Spectroscopy. *Nanostruct. Mater.* **1999**, *11*, 1181−1193.

(14) Sitar, Z.; Smith, L. L.; Davis, R. F. Interface Chemistry and Surface Morphology in the Initial Stages of Growth of GaN and AlN on α-SiC and Sapphire. *J. Cryst. Growth* **1994**, *141*, 11−21.

(15) Bertaud, T.; Sowinska, M.; Walczyk, D.; Thiess, S.; Gloskovskii, A.; Walczyk, C.; Schroeder, T. In-Operando and Non-Destructive Analysis of the Resistive Switching in the Ti/HfO_2/TiN-Based System by Hard X-ray Photoelectron Spectroscopy. *Appl. Phys. Lett.* **2012**, *101*, No. 143501.

(16) Soler, J. M.; Artacho, E.; Gale, J. D.; García, A.; Junquera, J.; Ordejón, P.; Sánchez-Portal, D. The SIESTA Method for Ab Initio Order-N Materials Simulation. *J. Phys.: Condens. Matter* **2002**, *14*, 2745−2779.

(17) Perdew, J. P.; Burke, K.; Ernzerhof, M. Generalized Gradient Approximation Made Simple. *Phys. Rev. Lett.* **1996**, *77*, 3865−3868.

(18) Adam, J.; Rogers, M. D. The Crystal Structure of ZrO_2 and HfO_2. *Acta Crystallogr.* **1959**, *12*, 951.

(19) Hann, R. E.; Suitch, P. R.; Pentecost, J. L. Monoclinic Crystal Structures of ZrO_2 and HfO_2 Refined from X-ray Powder Diffraction Data. *J. Am. Ceram. Soc.* **1985**, *68*, C285−C286.

(20) Gale, J. D. GULP: A Computer Program for the Symmetry-Adapted Simulation of Solids. *J. Chem. Soc., Faraday Trans.* **1997**, *93*, 629−637.

(21) Gale, J. D.; Rohl, A. L. The General Utility Lattice Program (GULP). *Mol. Simul.* **2003**, *29*, 291−341.

(22) Makov, G.; Payne, M. C. Periodic Boundary Conditions in Ab Initio Calculations. *Phys. Rev. B: Condens. Matter Mater. Phys.* **1995**, *51*, 4014−4022.

(23) Rurali, R.; Cartoixá, X. Theory of Defects in One-Dimensional Systems: Application to Al-Catalyzed Si Nanowires. *Nano Lett.* **2009**, *9*, 975−979.

(24) Scopel, W. L.; da Silva, A. J. R.; Fazzio, A. Amorphous HfO_2 and $Hf_{1-x}Si_xO$ Via a Melt-and-Quench Scheme Using Ab Initio Molecular Dynamics. *Phys. Rev. B: Condens. Matter Mater. Phys.* **2008**, *77*, No. 172101.

(25) Broqvist, P.; Pasquarello, A. Oxygen Vacancy in Monoclinic HfO_2: A Consistent Interpretation of Trap Assisted Conduction, Direct Electron Injection, and Optical Absorption Experiments. *Appl. Phys. Lett.* **2006**, *89*, No. 262904.